Delft University of Technology

Third party risk modelling of Unmanned Aircraft System operations, with application to parcel delivery service

Blom, Henk A.P.; Jiang, Chenpeng; Grimme, Wouter B.A.; Mitici, Mihaela; Cheung, Yuk S.

Important note
To cite this publication, please use the final published version (if applicable).
Please check the document version above.

Third party risk modelling of Unmanned Aircraft System operations, with application to parcel delivery service

Henk A.P. Blom [a],[*], Chenpeng Jiang [a], Wouter B.A. Grimme [a], Mihaela Mitici [a], Yuk S. Cheung [b]

[a] *Delft University of Technology, the Netherlands*
[b] *Netherlands Aerospace Centre NLR, the Netherlands*

ARTICLE INFO

ABSTRACT

Commercial aviation distinguishes three indicators for third party risk (TPR): i) Expected number of ground fatalities per aircraft flight hour; ii) Individual risk; and iii) Societal risk. The latter two indicators stem from TPR posed to population by operation of hazardous installations. Literature on TPR of Unmanned Aircraft System (UAS) operations have focused on the development of the first TPR indicator. However the expected increase of commercial UAS operations requires an improved understanding of third party risk (TPR). To support such improvement, this paper extends the existing TPR model for UAS operations with societal and individual risk indicators. The extension is developed both at modelling level and at assessment level. Subsequently the extended approach is applied to a hypothetical UAS based parcel delivery service in the city of Delft. The results obtained for the novel UAS TPR indicators show that this aligns commercial UAS operations with land use policies and standing TPR regulation for airports and hazardous facilities.

1. Introduction

An Unmanned Aircraft (UA) is an aircraft which is intended to operate with no pilot on board. A UA is either piloted from the ground or is autonomous. When piloted from the ground the UA and associated ground elements are referred to as an Unmanned Aircraft System (UAS) [1]. UAS have the ability to virtually replace manned aircraft and aerial platforms in many applications due to the considerable cost savings for not having to fly a helicopter or airplane with associated crew and fuel costs or transportation of a heavy aerial platform. The future possibilities are endless: imagine flying taxis, parcel delivery, medical aid; the list goes on and on. Because the safety risks of these UAS based operations are not well understood, under current regulations such commercial UAS operations over rural areas are not allowed [2,3]. To manage the future risk of commercial UAS operations over an urban area there is a need for models of third party risk (TPR) posed to persons on the ground by a large number of UA flights per annum.

For conventional aviation, third party risk (TPR) models have been well developed [4,5,6]. These models allow to assess changes in risk posed to persons on the ground due to changes in the amount of flights, new departure/arrival routes, the impact of a new airport, the risk of constructing a residential building in a certain area, etc. TPR models of conventional aviation are typically quantified using statistical analysis

of large scale collected incident and accident data. Because sufficient statistical incident/accident data is not available for UA flights, TPR analysis of UA flights is largely based on prospective models. Modelling ground TPR of a UAS operation involves an off-nominal UAS behaviour model, an off-nominal UA flight descent model, and a ground crash impact consequence model. The latter model captures population density, crash impact area, shelter and injury effects. Weibel and Hansman [7] show that the large range of UA types affects each of these model elements. Clothier and Walker [8] identifies and evaluates safety objectives of UAS operations. Dalamagkidis et al. [9] provides an in-depth overview of the spectrum of research issues in integrating UAS in the National Airspace System. Lum and Waggoner [10] show that a key bottleneck for safe integration of UAS operations in the National Airspace System is the risk posed to persons on the ground in a metropolitan area (e.g. Seattle area). Melnyk et al. [11] provides literature reviews for each of the five terms in the product of this ground TPR model. Subsequently, [11] uses this accumulated knowledge for the assessment of prospectively calculated TPR per flight hour for flying various UA types over various population densities. Finally these prospectively calculated TPR per flight hour are compared against statistically calculated TPR per flight hour for manned aviation and each difference is translated into a requirement on UAS system failure rate, i. e. the rate of events that cause an inability to maintain coordinated

flight. For UAS operations in an urban area the derived requirement on UAS system failure rates range from 3.42×10^{-4} per flight hour for a mini UA (≤ 2 kg), to 2.01×10^{-8} per flight hour for a heavy UA (> 4550 kg).

The potential of commercial use of small UAS for various applications has directed further development of TPR modelling and simulation. For small fixed-wing UAS, Rudnick-Cohen et al. [12,13], Bertrand et al. [14] and La Cour-Harbo [15,16] develop MC simulation approaches to evaluate the crash location density and its effect on ground TPR. [16] also extends this to small helicopter UA flights. Monte Carlo simulation of crash location density of a multi-rotor UA flight poses complementary challenges. Foster and Hartman [17] conduct large scale simulations of a high fidelity model of multi-rotor UA behaviour under different propulsion failures. Under abrupt power failure, the resulting tumbling mode descend yields a near-ballistic trajectory. Under a cascading power failure the multi-rotor UA enters into erratic transition dynamics and an out-of-control descent. In order to make UA behaviour under failure conditions better predictable, Cunningham et al. [18] develops a model of controlled termination of an anomaly UA flight. This creates a near-vertical descent by putting the UA in a sustained condition of high angle of attack and high drag using pro-spin controls. Ancel et al. [19] adopts the latter model for ground TPR assessment of a small multi-rotor UA flight. La Cour-Harbo [20] models ballistic descent of small UAs. Primatesta et al. [21] uses these TPR models for real-time navigation of a small UA flight such that it approximately minimizes TPR in flying over an urban area.

The above mentioned studies consider TPR from a UA flight perspective. However, there also is a need to assess TPR from a population perspective, i.e. to assess the accumulated TPR that is posed to a population by a UAS based operation that conducts a large number of flights per annum. For commercial aviation this population perspective on TPR has been well developed in the form of individual and societal risk [4,5,6]. The objective of this paper is to extend the existing TPR model for UAS flights with individual and societal risk models that can be assessed through conducting MC simulations. The existing and novel TPR approaches are subsequently compared for a hypothetical UAS-based parcel delivery service.

This paper is organized as follows. Section 2 reviews existing TPR models for commercial aviation and for UAS operations. Section 3 extends these TPR models to UAS operations involving a large number of flights per annum over an urban area. Section 4 develops a Monte Carlo simulation method for the assessment of the extended TPR models. Section 5 develops a model for UAS based parcel delivery service in the city of Delft. Section 6 evaluates the TPR risks for this parcel delivery service using the model and simulation approach from Sections 3 and 4. Section 7 draws conclusions and identifies follow-on research.

2. TPR models in aviation research literature

2.1. TPR models for commercial aviation

In commercial aviation almost all fatalities concern persons onboard aircraft. This explains why in commercial aviation the TPR indicator of the expected number of ground fatalities per flight hour plays a marginal role. Instead, commonly used indicators for TPR in commercial aviation are defined from a ground population perspective; these are individual risk and for societal risk the FN curve and collective risk [4,5,6].

Individual risk $R_I(y)$ of commercial air transport is defined as: "The probability that an average unprotected person, who resides permanently at ground location y, would get killed or fatally injured due to the direct consequences of an aircraft accident during a given annum." Notice that by its definition, the individual risk indicator $R_I(y)$ does not make any difference if a ground location y is in a rural area or in the center of a city. Individual risk defines risk contours on a location map that are used for zonal policies regarding any current or future use of a given area that is exposed to non-negligible Individual risk levels.

The mathematical characterization of Individual risk of $R_I(y)$ satisfies [5]:

$$R_I(y) = \sum_d [N_d P(C|d) p_s(y|d) \, |A(d)| \, P(F|y \in A(d))] \tag{2.1}$$

where N_d is the annual number of flights of type d, $P(C|d)$ is the accident probability model, $p_s(.|d)$ is the crash location model, $|A(d)|$ is the crash area size, and $P(F|y \in A(d))$ is the fatality model. Formal definitions of these five terms are given in the box below.

Formal definitions of the terms in equations (2.1-2.2).

$N_D =$ number of flights of type d per annum flying in area Y.

$P(C|d) =$ conditional probability that type d flight crashes to ground.

$p_s(.|d) =$ pdf of the crash location of a type d flight.

$|A(d)| =$ size of the crash impact area $A(d)$ of a type d flight.

$P(F|y \in A(d)) =$ conditional probability that crash of a type d flight is fatal for an unprotected average person in crash impact area $A(d)$.

$n_F^d =$ number of 3rd party fatalities due to an accident of a type d flight.

To capture societal risk the FN curve $R_{FN}(n)$ is defined as [22]: "The probability that a group of n or more third party persons will be killed or fatally injured due to the direct consequences of an aircraft accident during a given annum.", i.e. for $n \geq 1$:

$$R_{FN}(n) = 1 - \prod_d \left[1 - P\{n_F^d \geq n\}\right]^{N_d} \cong \sum_d \left[N_d P\{n_F^d \geq n\}\right] \tag{2.2}$$

with n_F^d the number of third party fatalities due to an accident of a type d flight. Some literature sources, e.g. [6] refer to "*more than n*", which defines $R_{FN}^>(n)$ as $R_{FN}^>(n) = R_{FN}(n+1)$, for $n \geq 0$.

Safety regulation of hazardous installations in various countries typically adopts an $R_{FN}(n)$ limiting criterion of the following form, e.g. [6]:

$$R_{FN}(n) < C/n^\alpha \tag{2.3}$$

where α is the steepness of the limit line and C a constant that determines the position of the limit line. A steepness $\alpha = 1$ is called risk neutral (e.g. in UK); a steepness $\alpha = 2$ is called risk averse (e.g. in the Netherlands). In the latter case larger accidents are weighted more heavily and are thus only accepted with a relatively lower probability. Within Europe there is an effort to develop a common approach in setting values for C and α [23].

Another societal risk indicator is Collective risk R_C, which is defined as

$$R_C = E\{n_F\} \tag{2.4}$$

where n_F is the number of persons on the ground in a given area Y that are killed or fatally injured due to the direct consequences of aircraft flight accidents during a given annum [24]. Collective risk R_C is known to be equal to a summation over the FN-curve, e.g. [22]:

$$R_C = \sum_{n=1}^{\infty} R_{FN}(n) = \sum_{n=0}^{\infty} R_{FN}^>(n). \tag{2.5}$$

To express the relation between Collective risk and Individual risk common practice is to assume that people on the ground are unprotected to a crash of a commercial aircraft. Under this assumption [22] shows:

$$R_C = \int_Y R_I(y)\rho(y)dy \qquad (2.6)$$

where $\rho(y)$ is the population density as a function of crash center location y, and Y is the area that may be affected by aircraft accidents.

2.2. TPR models for UAS operations

Literature on TPR models for UAS operations has focused on $R^i_{Cground}$ $= E\{n^{UAS}_{F,i}\}$, where $n^{UAS}_{F,i}$ is the number of persons on the ground that are killed or fatality injured due to the i-th UA flight colliding to the ground, This has resulted in the following characterization [14,19]:

$$R^i_{Cground} = E\left\{n^{UAS}_{F,i}\right\} = \int_Y R^i_I(y)[1 - P(S|y,i)]\rho(y)dy \qquad (2.7)$$

where $R^i_I(y)$ is the individual risk for an unprotected person at location y posed by the i-th flight, $P(S|y,i)$ is the shelter protection model and $\rho(y)$ is the population density in the area Y considered.

The characterization of $R^i_I(y)$ in UAS literature satisfies [14, 16, 21]:

$$R^i_I(y) = \sum_{e \in E}[P(e|i)p_s(y|i,e)|A(d_i,e)|P(F|y \in A(d_i,e))] \qquad (2.8)$$

where E is the set of possible crash event types, $P(e|i)$ is ground crash probability, $p_s(.|i,e)$ is the crash location model, $|A(d_i,e)|$ is the size of the crash impact area, $P(F|y \in A(d_i,e))$ is the unprotected fatality model.

Formal definitions of the terms in Eqs. (2.7-2.8).

$R^i_I(y)$ = probability that an unprotected average person at ground location y is killed or fatally injured due to ground crash by ith flight.

$P(S|y,i)$ = probability that a person at location y is sheltered against a crash of the ith UA flight.

$\rho(y)$ = population density as a function of location y.

$P(e|i)$ = probability of event type e ground crash by ith UA flight.

$p_s(.|i,e)$ = pdf of crash location of ith UA flight due to event type e.

$|A(d_i,e)|$ = size of event type e crash impact area of UA type d_i.

$P(F|y \in A(d_i,e)) = P(F|y \in A(d_i,e),d_i,e)$ = probability that a crash of a UA flight of type d_i due to event type e is fatal for an unprotected average person in the crash impact area $A(d_i,e)$.

2.3. Submodels developed in literature

The difference between Eq. (2.7) and Eq. (2.6) is that (2.7) includes shelter protection and (2.6) not. The main difference between Eq. (2.8) and Eq. (2.1) is that Eq. (2.1) accumulates over all annual flights, and (2.8) not. Another difference is that Eq. (2.8) differentiates regarding types of flight and crash event, while (2.1) differentiates regarding type of flight only. In spite of the similarities there are significant differences in the approaches used for the numerical evaluation of the product terms in these equations. For commercial aviation the numerical evaluation of (2.1-2.2) is largely based on statistical modelling of accident data from the past [5]. Because for future UAS operations such accident data is not available, use has to be made of dedicated submodels.

An event $e \in E$ types consists of two indicators: e_H for the hazard causing the UA crash and e_θ the mode of the descend path to the ground. La Cour-Harbo [16] distinguishes four e_θ modes: ballistic descend, uncontrolled glide, parachute descend, and fly-away. For a quadcopter [17] distinguishes several complementary e_θ modes. The e_H types include all UAS system failures, i.e. events that would cause an inability to maintain coordinated flight [11]. UAS system failure causes may vary from human error, unexpected adverse weather, or collision with a bird, a building or with another UA. Weibel and Hansman [7], Lum et al. [25], Dalamagkidis et al. [9], Melnyk et al. [11] consider effects of system failures of UA flights over areas with homogeneous population density. The homogeneous population density assumption simplifies the assessment of equations (2.7-2.8) in the sense that there is no need to take the shape of crash location density $p_s(.|i,e)$ into account.

Melnyk et al. [11] provides a very good review of the various submodels needed to evaluate Eqs. (2.7-2.8). More recent studies have further extended the submodels for location density $p_s(.|i,e)$ and event types $P(e|i)$. For the latter, Barr et al. [26] developed a Bayesian Belief Net, Bertrand et al. [14] developed a Fault Tree model, while Kim [27, 28] and La Cour-Harbo and Schiøler [29] developed collision probability models between UAs and between a UA and low-flying General Aviation. For the evaluation of the location density $p_s(.|i,e)$ in Eq. (2.8), probabilistic models and MC simulation methods have also been developed for fixed wing UA [12-15], for helicopter [30,16], and for multi-rotor UA [17,18,20].

3. Novel TPR indicators for UAS operation

For a commercial UAS operation involving many flights per annum, there is need for novel TPR indicators from a population perspective. Based on the TPR indicators in Section 2.1, this section elaborates for UA crash to the ground: Individual risk $R^{UAS}_I(y)$ and societal indicators FN-curve R^{UAS}_{FN} and Collective ground risk $R^{UAS}_{Cground}$ in Sections 3.1 and 3.2 respectively. In Section 3.3 impact velocity is incorporated.

Formal definitions of the terms in Eqs. (2.7-2.8) are given in the box below.

$R^i_I(y)$ = probability that an unprotected average person at ground location y is killed or fatally injured due to ground crash by ith flight.

$P(S|y,i)$ = probability that a person at location y is sheltered against a crash of the ith UA flight.

$\rho(y)$ = population density as a function of location y.

$P(e|i)$ = probability of event type e ground crash by ith UA flight.

$p_s(.|i,e)$ = pdf of crash location of ith UA flight due to event type e.

$|A(d_i,e)|$ = size of event type e crash impact area of UA type d_i.

$P(F|y \in A(d_i,e)) = P(F|y \in A(d_i,e),d_i,e)$ = probability that a crash of a UA flight of type d_i due to event type e is fatal for an unprotected average person in the crash impact area $A(d_i,e)$.

3.1. Individual risk of UAS operations

Individual risk $R_I^{UAS}(y)$ due to possible crashes to the ground by a UAS operation involving multiple flights per annum is defined as: "The probability that an average unprotected person, who resides permanently at ground location y, would get killed or fatally injured due to the direct consequences of a ground crash by a UA flight during a given annum."

Aalmoes et al. [31] proposed a version of Eq. (2.1) as the basic model for Individual risk $R_I^{UAS}(y)$. To take advantage of the TPR model development in literature, it has an advantage to connect the above Individual risk definition to equations in Section 2.2 and the developed sub-models in Section 2.3. To make the connection N UA flights per annum over the area Y are assumed. Then the probability of a person at location y being missed by all N UA flights per annum equals the product over the miss probabilities $[1 - R_I^i(y)]$ for the $i = 1, ., N$ UA flights. Hence, Individual risk $R_I^{UAS}(y)$ satisfies:

$$R_I^{UAS}(y) = 1 - \prod_{i=1}^{N}\left[1 - R_I^i(y)\right] \tag{3.1}$$

with $R_I^i(y)$ satisfying Eq. (2.8). Often $R_I^{UAS}(y) \ll 0.1$, then Eq. (3.1) can be approximated by $R_I^{UAS}(y) \cong \sum_{i=1}^{N} R_I^i(y)$.

3.2. FN-curve and collective ground risk of UAS operations

For a UAS operation involving multiple flights per annum over an area Y the FN curve $R_{FN}^{UAS}(n)$ is defined as the "The probability that in an area Y a group of n or more third party persons will be killed or fatally injured due to the direct consequences of ground crashes by UA flights during a given annum", i.e. for $n \geq 1$:

$$R_{FN}^{UAS}(n) = 1 - \prod_{i=1}^{N}\left[1 - P\{n_F^i \geq n\}\right] \cong \sum_{i=1}^{N}\left[P\{n_F^i \geq n\}\right] \tag{3.2}$$

where n_F^i is the number of persons on the ground that are killed or fatally injured due to a ground crash of the i-th UA flight. In contrast to commercial aviation ground crashes, for almost all UAS ground crashes $n_F^i \leq 1$. This implies that the FN-curve $R_{FN}^{UAS}(n)$ for UAS will decrease more steeply with increasing n than the FN-curve $R_{FN}(n)$ does for commercial aviation.

Collective ground risk $R_{Cground}^{UAS}$ of a UAS operation involving multiple flights per annum over an area Y is defined as: "The expected number of persons on the ground in a given area Y that are killed or fatally injured due to the direct consequences of ground crashes by flights of the UAS operation during a given annum". Hence for a UAS operation conducting N flights per annum:

$$R_{Cground}^{UAS} = \sum_{i=1}^{N} R_{Cground}^i \tag{3.3}$$

where $R_{Cground}^i$ satisfies (2.7). Also for a UAS operation, collective ground risk equals the summation over the FN-curve, i.e.

$$R_{Cground}^{UAS} = \sum_{n=1}^{\infty} R_{FN}^{UAS}(n) \tag{3.4}$$

Adopting FN requirement (2.3) also on $R_{FN}^{UAS}(n)$ and substituting this into (3.4) yields the following bound on collective ground risk

$$R_{Cground}^{UAS} < C \sum_{n=1}^{\infty} \frac{1}{n^\alpha} = C\,\zeta(\alpha) \tag{3.5}$$

with $\zeta(.)$ the Riemann zeta function [32, p.807]. For $\alpha = 2$ this yields $\zeta(2) = \pi^2/6$. For $\alpha = 1$ this yields $\zeta(1) = \infty$, which means that the FN-curve requirement does not imply a bound on UAS collective ground

risk $R_{Cground}^{UAS}$. Because the FN-curve for UAS operations will be steep in Eq. (3.5) α should always be larger than 1, hence $\zeta(\alpha)$ is bounded.

3.3. Incorporating impact velocity

The last term in Eq. (2.8), i.e. $P(F|y \in A(i,e))$, depends on the kinetic energy $1/2mv^2$ of the i-th UA flight at the moment of impact of crash type e. In evaluating this term, common practice is to adopt a certain impact velocity, e.g. [14,16,21]. Because the impact velocity may assume values from a set V, a better approach is to incorporate the impact velocity v in $P(F|y \in A(i,e))$. To do so we make use of the law of total probability:

$$P(F|y \in A(i,e)) = \int_V P(F,v|y \in A(i,e))dv \tag{3.6}$$

Application of conditional probability to $P(F,v|y \in A(i,e))$ yields:

$$P(F|y \in A(i,e)) = \int_V P(F|v,y \in A(i,e))p(v|y \in A(i,e))dv \tag{3.7}$$

where $p(v|y \in A(i,e))$ is the conditional density of impact velocity v given $y \in A(i,e)$ and $P(F|v,y \in A(i,e))$ is "The conditional probability that an average person at a location in the crash impact area $A(i,e)$ of the i-th UA flight under event e, will be killed or fatally injured, given the velocity v of the UA at the moment of crash." Rudnick-Cohen et al. [13] and Haartsen et al. [30] propose MC simulation to evaluate $p(v|y \in A(i,e))$.

4. MC simulation of TPR models for UAS operation

This section specifies the steps to numerically evaluate the novel TPR models for Individual risk and Collective risk. Section 4.1 explains the Monte Carlo simulation steps. Section 4.2 explains the steps for the evaluation of Individual risk. Section 4.3 explains the follow-on steps for the evaluation of Collective ground risk, both for each individual flight and for the population in the area considered.

4.1. Monte Carlo simulation approach

We consider a UAS based operation conducting N flights per annum over an area Y, using different types of UAs. We assume the volume of airspace used by these N flights is separated from airspace in use by Commercial Air Transport, General Aviation and Urban Air Mobility operations. The objective is to estimate Individual risk $R_I^{UAS}(y)$ for each position $y \in Y$.

A straightforward way to accomplish this is to first conduct a Monte Carlo simulation for the generation of N nominal flight plans, and subsequently to conduct a Monte Carlo simulation of K flights for each of these N nominal flight plans. This approach would lead to a MC simulation consisting of simulating NK flights. However, for ground TPR assessment it suffices to only simulate the fraction of those flights that are subject to a failure event leading to a ground crash. Elaboration of this approach for MC based assessment of Individual risk yields the following series of Steps.

Step 0: Determine N delivery locations and UA types

Draw N independent delivery destination locations in the area Y according to the population density $\rho(y)$. Subsequently draw for each of these N destinations a delivery payload according to a known probability density of these payloads. Based on the i-th payload sample, select for the i-th flight a suitable UA type d_i from those in use by the parcel delivery service.

Step 1: Determine nominal flight plans for each of the N delivery flights

Determine for each of the N parcel delivery flights (outbound and inbound), a series of 3-dimensional waypoints, the nominal states $x_t^{i,nom}$, $t \in [0, T_i^{nom}]$, of a 4-dimensional nominal flight path through these waypoints, of nominal duration T_i^{nom}, $i = 1,.., N$. The components of the nominal state $x_t^{i,nom}$ are 3D position $s_t^{i,nom}$, 3D velocity $v_t^{i,nom}$ and mode $\theta_t^{i,nom}$.

Step 2: Evaluate ground crash probability. Calculate for each of the N flights and each $e \in E$ the probability of crash:

$$P(e|i) = 1 - \exp\left\{ - \int_0^{T_i^{nom}} \lambda_{i,e}(t)dt \right\} \tag{4.1}$$

with $\lambda_{i,e}(t)$ the rate of event e to happen at moment t during the i-th flight. A relevant event type for which $\lambda_{i,e}(t)$ is not constant in time is mid-air collision rate of the i-th UA flight with any of the other UA flights [28].

Step 3: Simulation of UA flights that crash.

Conduct for each of the N flights and each $e \in E$ a Monte Carlo simulation consisting of K_i runs that crash to the ground, i.e. for $k = 1,...,$ K_i. The typical value for $K_i = \lceil T_i^{nom} \rceil$. For each (i,e) this is done in substeps 3.1-3.3:

Substep 3.1: Draw K_i independent event time samples $t_e^{i,k}$ from the density $\lambda_{i,e}(t)$ on the time interval $[0, T_i^{nom}]$.
Substep 3.2: Simulate for the i,k-th flight, for each $e \in E$ the UA state at moment of failure event $t_e^{i,k}$. The UA state components to be generated are 3D position $s_{te}^{i,k}$, 3D velocity $v_{te}^{i,k}$ and attitude $\theta_{te}^{i,k}$:

$$s_{te}^{i,k} = s_{te}^{i,nom} + \varepsilon_{te}^s \tag{4.2a}$$

$$v_{te}^{i,k} = v_{te}^{i,nom} + \varepsilon_{te}^v \tag{4.2b}$$

$$\theta_{te}^{i,k} = e_\theta \tag{4.2c}$$

where e_θ is the applicable non-nominal descend mode component of e, ε_{te}^s is a Gaussian navigation error in horizontal and vertical position with standard deviations (σ_H^s, σ_V^s), and ε_{te}^v is an independent Gaussian deviation from nominal velocity with standard deviations (σ_H^v, σ_V^v).

Substep 3.3: For each e_θ that applies to the i,k-th flight, simulate the non-nominal descend on the time interval $[t_e^{i,k}, t_{c,e}^{i,k}]$, i.e. from $t_e^{i,k}$ until moment of ground crash $t_{c,e}^{i,k}$. This yields the UA state $x_{c,e}^{i,k}$, at moment $t_{c,e}^{i,k}$. The applicable differential equations to be used depend of the event type e and the desired model fidelity. As an example we provide the differential equations from [20] for a ballistic descent model of a quadcopter:

$$\dot{s}_t = v_t \tag{4.3a}$$

$$\dot{v}_t = Col\{0, 0, g\} - C_D A_S \varrho_t \parallel v_t - w_t \parallel (v_t - w_t) \big/ 2m \tag{4.3b}$$

where g is the gravitational constant, C_D is the drag coefficient, A_s the surface area, m is the mass of UA with payload, ϱ_t and w_t are air density and wind velocity vector at moment t, respectively. The latter two are considered to be functions of 3-dimensional position s_t. Rather than adding the wind effect in the differential equation for the position as is done in [18], w_t is incorporated in the drag component of the acceleration [33].

4.2. Evaluation of individual risk

The results from the Monte Carlo simulation approach of Section 4.1 are now used to estimate Individual risk in a number of steps.

Step 4: Evaluation of the crash location model.

Calculate for each $e \in E$ and each $i = 1,.., N$ the estimate $\widehat{p}_s(y_j|i,e)$ of the local hit density $p_s(y_j|i,e)$ for an arbitrary location y_j in grid cell G_j in area Y:

$$\widehat{p}_s(y_j|i,e) = \widehat{P}(j|i,e) \big/ |G_j| \tag{4.4a}$$

where $|G_j|$ is the area size of the j-th grid cell and $\widehat{P}(j|i,e)$ the estimated probability that the simulated crash locations $s_{c,e}^{i,k}$, $k = 1,.., K_i$, is in grid cell G_j, i.e.

$$\widehat{P}(j|i,e) = \sum_{k=1}^{K_i}\left[1\left[s_{c,e}^{i,k} \in G_j \right] \right] \big/ K_i \tag{4.4b}$$

where $s_{c,e}^{i,k}$ is the simulated UA position at crash moment $t_{c,e}^{i,k}$, and 1 is an indicator function, i.e. $1[true] = 1$, $1[false] = 0$.

Step 5: Evaluation of unprotected fatality model.

To estimate $\widehat{P}(F|j,i,e)$ of $P(F|y \in A(i,e))$ in Eq. (3.7) we evaluate for each j,i,e for which $\widehat{P}(j|i,e) > 0$:

$$\widehat{P}(F|j,i,e) = \widehat{P}(F,j|i,e) \big/ \widehat{P}(j|i,e) \tag{4.5a}$$

with nominator

$$\widehat{P}(F,j|i,e) = \sum_{k=1}^{K_i}\left[1\left[s_{c,e}^{i,k} \in G_j \right] P\left(F \middle| v_{c,e}^{i,k}, s_{c,e}^{i,k} \in A(i,e) \right) \right] \big/ K_i \tag{4.5b}$$

Step 6: Evaluation of Individual risk per UA flight.

To estimate $\widehat{R}_I^i(y)$ of $R_I^i(y)$ in Eq. (2.8) we evaluate for an arbitrary location y_j in grid cell G_j, for each i-th flight:

$$\widehat{R}_I^i(y) = \sum_{e \in E}\left[P(e|i)\, \widehat{p}_s(y_j|i,e)\, |A(i,e)|\, \widehat{P}(F|j,i,e) \right] \tag{4.6}$$

Step 7: Evaluation of Individual risk. Calculate the estimated individual risk for an arbitrary location y_j in grid cell G_j following Eq. (3.1):

$$\widehat{R}_I^{UAS}(y_j) = 1 - \prod_{i=1}^{N}\left[1 - \widehat{R}_I^i(y) \right] \tag{4.7}$$

Step 8: Compare, for each j, $\widehat{R}_I^{UAS}(y_j)$ versus applicable threshold values of acceptable level of Individual risk for commercial aviation around an airport. The applicable threshold in UK and The

Netherlands for Individual risk is 10^{-6} per annum [34,35]. If $\widehat{R}_I^{UAS}(y_j)$ is higher, then evaluate what this means to the UAS operation considered.

4.3. Evaluation of collective ground risk by Monte Carlo simulation

For the evaluation of Collective ground risk, population density has to be taken into account as well as shelter protection using Eqs. (2.7) and (3.3). This yields the following series of additional steps.

Step 9: Assess the population map $\widehat{\rho}_j = \rho(y_j)|G_j|$ for each grid cell G_j.
Step 10 Assess for each grid cell G_j the probability of shelter protection against a ground crash of the i-th UA flight. This yields estimated shelter probability $\widehat{P}(S|j,i)$ for each j,i.
Step 11: Estimate Collective ground risk per flight. Calculate $\widehat{R}_{Cground}^i$, i.e. the estimated Collective ground risk per UA flight in area Y using Eq. (2.7):

$$\widehat{R}_{Cground}^i = \sum_j \left[\widehat{R}_I^i(y) \left[1 - \widehat{P}(S|j,i) \right] \widehat{\rho}_j \right] \qquad (4.8)$$

Step 12: Estimate Collective ground risk per flight hour for each flight. Calculate, for each i, the collective ground risk per UA flight hour $\widehat{R}_{Cground}^i / T_i^{nom}$, and present the results for N flights in a histogram.
Step 13: Verify if a part of this empirical density passes an applicable threshold level. For example, [3] proposed a threshold of 10^{-6} fatal injuries on the ground per UA flight hour. For the part above the threshold it has to be evaluated what this means for the UAS operation considered.
Step 14: Calculate the estimated Collective ground risk using Eq. (3.3):

$$\widehat{R}_{Cground}^{UAS} = \sum_{i=1}^N \widehat{R}_{Cground}^i \qquad (4.9)$$

Step 15: Compare the estimated Collective ground risk versus an applicable threshold level of Collective ground risk. In Eq. (3.5) such a threshold has been based on requirements posed on an FN-curve

[34,35]. If the risk is higher, then evaluate what this means to the UAS operation considered.

5. Parcel delivery service by UAS

In this section we specify a hypothetical scenario of a UAS based parcel delivery service in the city of Delft. In Section 5.1 the hub location is shown together with the population and service radius while in Section 5.2 the number of UA flights, parcel weight and parcel delivery locations are determined. In Section 5.3 the wind distribution used for the scenario simulation is addressed. The UAS specifications are discussed in Section 5.4, and the flight profile of a parcel delivery UA is shown in Section 5.5.

5.1. Hub location, population and service area

For the UAS delivery area Y the city Delft is chosen. The hub is at an industrial area within the city, and the service radius is 2.5 km. An overview of the hub location, service radius and population distribution can be seen in Fig. 1. The number of people living within the service area is estimated to be 120,838 using census data of Delft [36].

5.2. Number of UA flights, parcel weight and delivery locations

To estimate the number of UA flights per annum, we firstly estimate the number of parcel deliveries per person per year. The latter has been done by [37] for UAS based deliveries in Paris, France. The estimated number of deliveries per person per year is assumed to be 70% of the 2018 number of parcels delivered in Paris. With 12.3 million people and an estimated 161 million eligible parcels for the year 2018, that results in about 13.1 parcels per person per year. Based on the census data for the Delft area, this yields $N = 1,582,985$ UAS based deliveries per year within the service radius in Fig. 1.

The density of the parcel delivery locations is assumed to be the same as the population density within the delivery circle in Fig. 1. The weight of the parcels is assumed to be uniformly distributed between 0.1 and 2.2 kg.

5.3. Wind distribution

For the scenario vertical wind is assumed to be zero, and horizontal wind is based on actual wind measurements. Hourly wind data over the years 2013–2018 is used from the wind measurement post of Rotterdam
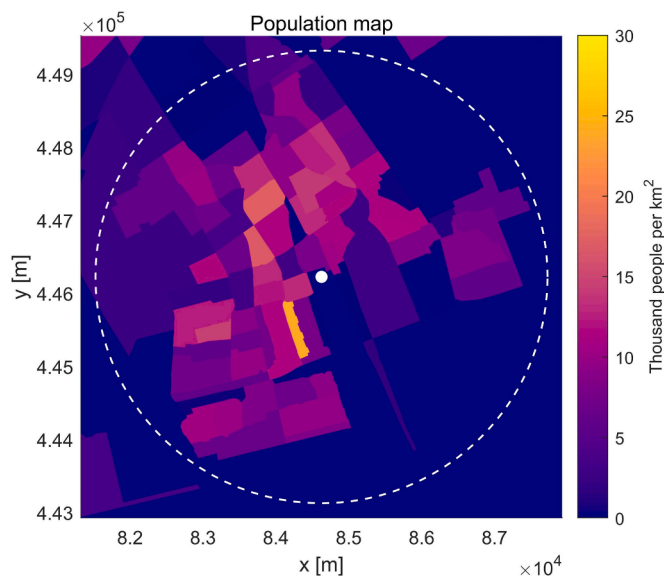

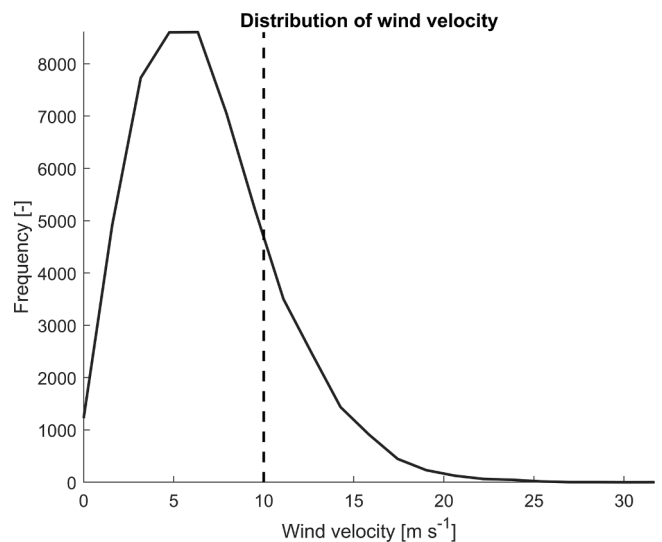**Fig. 1.** Hub location, service radius and population density [35].

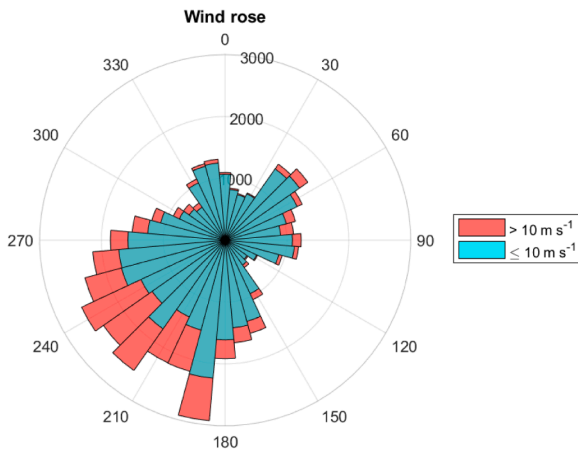**Fig. 2.** w^s velocity distribution at 120 m based on converted wind data; parcel delivery is stopped if w^s is above 10 m/s.

Fig. 3. Wind rose of w^s velocity based on converted wind data.

Table 1
Adopted UAS parameter values.

	UA$_{Small}$	UA$_{Large}$	Units
m_{drone}	2.7	6.0	kg
$m_{payload}$	1	3	kg
Range	15	25	km
v_{cruise}	12	20	m s^{-1}
v_{ascent}	7.5	10	m s^{-1}
$v_{descent}$	6	8	m s^{-1}
C_D	N(0.7,0.2)	N(0.7,0.2)	
A_s	0.1	0.4	m^2
Planform area	1.1	3.9	m^2
σ_H^s	3.68	3.68	m
σ_V^s	7.65	7.65	m
σ_H^v	2.0	2.0	m/s
σ_V^v	2.0	2.0	m/s

[38]. The empirical wind vector w^e is measured over an open area at an altitude of 10 m. In order to compensate for the altitude and air stability measurement conditions, [33] has conversed this to the applicable height under an air stability exponent for an average urban area. The resulting empirical distribution of w^s at 120 m altitude is shown by the wind velocity distribution in Fig. 2 and the wind rose in Fig. 3. It is furthermore assumed that UA parcel delivery flights do not start when the expected wind velocity at cruise level is higher than $\| w_{max} \| = 10$ m s^{-1}.

5.4. Hypothetical UA specifications and UA selection

Two types of UAs are used for the parcel deliveries: a smaller UA with

a payload of up to 1 kg and a larger UA with a payload of up to 3 kg. For every parcel that must be delivered, the smallest UA that can deliver the parcel in terms of both payload and range is selected. A full list of parameter values for both UAs are given in Table 1.

The hypothetical larger UA in the parcel delivery scenario is based on the "MicroUAS MD4-3000 quadcopter UA" [39] which was used as an example for a delivery in the METROPOLIS report [40]. The hypothetical smaller UA is based on the MD4-1000 quadcopter from the same company for the sake of consistency [41]. The descent velocity is set to 80% of the ascent velocity to prevent vortex ring state of the rotors [42]. It is assumed that the drag coefficient C_D satisfies the probabilistic model adopted by [20] for ballistic descent of DJI Phantom 4. The latter has a symmetrical aerodynamic configuration that is similar to MD4-3000 and MD4-1000. The front area A_s is measured based on front images of MD4-3000 and of MD4-1000. Typically UA navigation is based on Global Positioning System, for which (σ_H^s, σ_V^s) values have been standardized under good satellite coverage [43]. For (σ_H^v, σ_V^v) values from [20] are adopted.

5.5. Flight profile of a parcel delivery UA

One delivery flight consists of outbound and inbound paths. Hence for each parcel delivery a nominal flight profile from the hub to the delivery location and back is determined. A one-way profile is depicted in Fig. 4. A UA with mass $m_{UA} + m_{payload}$ starts at the delivery hub, where it flies straight up (hover-ascent) with velocity v_{ascent} until it reaches altitude $h_{hover} = 50m$, where it transitions to a cruise-ascent, with horizontal velocity v_{cruise} an vertical velocity v_{ascent}. The UA continues this flight path until it reaches $h_{cruise}=120m$, where the UA transitions to a level cruise flight with velocity v_{cruise}. At some distance from the target, the UA transitions to a cruise-descent, with horizontal velocity v_{cruise} and vertical velocity $- v_{descent}$, until it reaches h_{hover} again. At that point, the UA transitions into a straight down path (hover-descent) with velocity $- v_{descent}$. During the return path the mass is m_{UA} and the flight profile is obtained in a similar way. Because $v_{ascent} \neq v_{descent}$ the return profile differs from the return profile, it rather is a mirror image. To avoid conflicts with outbound flights, return flights climb to a slightly higher level.

6. Monte Carlo simulation results

The aim of this section is to assess and compare for the hypothetical parcel delivery service of Section 5 the existing TPR indicator of Collective ground risk per flight (Section 2.2) and the two novel TPR indicators: Individual risk per annum (Section 3.1) and Collective ground risk per annum (Section 3.2). For this assessment the MC simulation method of Section 4 is used. First Section 6.1 describes the adopted TPR submodels. Then Section 6.2 presents the results for the existing TPR indicator. Subsequently Sections 6.3 and 6.4 present the results for the two novel TPR indicators. Section 6.5 compares the results obtained for the three TPR indicators, and addresses effects of model assumptions.
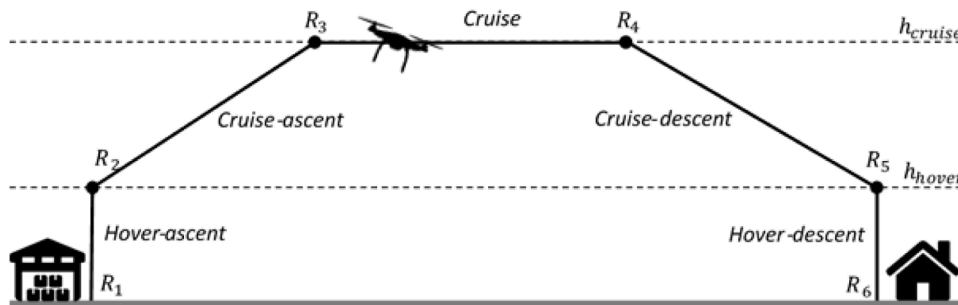

Fig. 4. One-way flight profile for a parcel delivery UA.

6.1. TPR submodels adopted in the MC simulation

The TPR submodels that remain to be selected concerns Eqs. (2.6-2.7). For operations by a mini UA over an urban area [11] derives a UAS system failure rate requirement of 0.342 per 1000 flight hour; the latter value we adopt, i.e. $\lambda_{i,H} = 3.42 \times 10^{-4}$ per hour, where the subscript H refers to all e_H that would cause a crash to the ground (due to inability to maintain coordinated flight). Regarding the mode e_θ of a quadcopter descend path to the ground we adopt the conservative assumption that the ballistic descent model of [20,33] applies (see substep 3.3).

For the probability of fatality, use is made of the Range Commanders Council [44] adopted Feinstein model:

$$P(F|y \in A(i,H),v) = Z\left(\frac{\ln E_{imp} - \ln a}{b}\right) \quad (6.1)$$

where Z is the cumulative standard normal distribution [9, p. 102]. $E_{imp} = m|v|^2/2$ is the kinetic energy of UA at moment of impact, with impact velocity vector v and with impact mass $m = m_{UA} + m_{payload}$ during outbound, or $m = m_{UA}$ during inbound. Hence Z defines an S-shaped curve that starts at probability zero for $E_{imp} = 0$, reaches probability ½ for $E_{imp} = a$ and asymptotically goes to probability 1 for large E_{imp}. Feinstein et al. [45] have used impact data to assess the mid-point value $a = 101.6$ Joule and standard deviation $b = 0.538$ of the effect of $\ln E_{imp}$.

The size of the crash impact area $|A(i,H)|$ is assumed to be equal to the size of the planform rectangle area of the ith flight. The rationale for selecting this relative small crash impact area is that a ballistic UA descent leads to hitting a human mainly on the head, and that the UA weight has less effect if the head is hit off-center, e.g. by one of the rotor engines.

Regarding the shelter model, a fixed probability value of shelter protection is assumed. For the USA, [11] provides statistical value for the time spent outdoors of 7.8 % and for the time spent in vehicle of 5.5%. To take into account that in The Netherlands cycles and mobility scooters are frequently used instead of cars, for Delft we adopt a value of 10% that persons are unprotected outdoors, i.e. $\widehat{P}(S|i,H) = 0.9$.

For the MC simulation, the adopted size of grid cells $|G_j| = 25 \ m^2$. The MC simulation took 6.1 hours on an ASUS RS700A-E9-RS4 with an AMD Epyc 7551 processor having 32 cores and 64 threads and 256 GB of RAM.
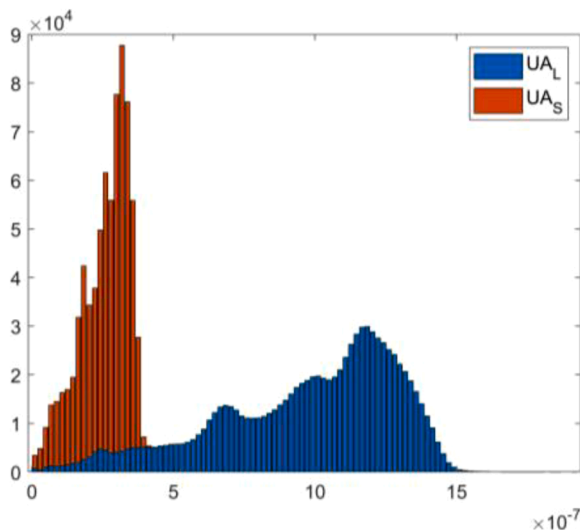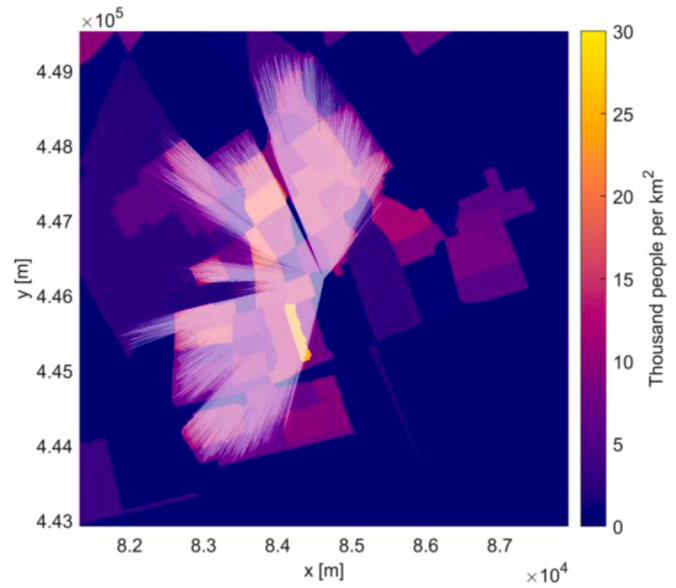

Fig. 6. UA Flight Paths with $\widehat{R}^i_{Cground}/T^{nom}_i > 10^{-6}$.

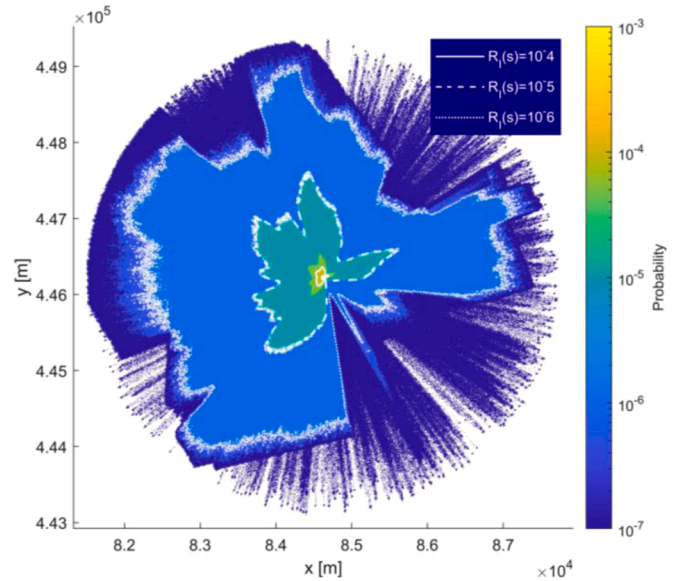**Fig. 7.** Individual risk $\widehat{R}^{UAS}_I(j)$ within the service are, with contours for $\widehat{R}^{UAS}_I(j) = 10^{-6}, 10^{-5}, 10^{-4}$.

6.2. Estimated collective ground risk per UA flight hour

In Step 12, for each of the N flights the collective ground risk per UA flight hour $\widehat{R}^i_{Cground}/T^{nom}_i$ is calculated. The results are presented in the form of a histogram in Fig. 5; this shows two increasing patterns with peaks at 3.2×10^{-7} and 1.2×10^{-6} stemming from flights by the small and large UA types respectively. The maximum value is 1.93×10^{-6} per flight hour; the mean value is 6.73×10^{-7} per flight hour.

For Step 13, the histogram in Fig. 5 to compare $\widehat{R}^i_{Cground}/T^{nom}_i$ against the applicable threshold value of 10^{-6} per UA flight hour. Although the mean value of $\widehat{R}^i_{Cground}/T^{nom}_i$ is clearly smaller than the threshold value of 10^{-6}, $\widehat{R}^i_{Cground}/T^{nom}_i > 10^{-6}$ for 497,401 of the 1,582,985 UA flights, i.e. 31.4%. The good news is that of these 31.4% of the UA

Fig. 5. Histogram of $\widehat{R}^i_{Cground}/T^{nom}_i$; blue = large UA, red = small UA.
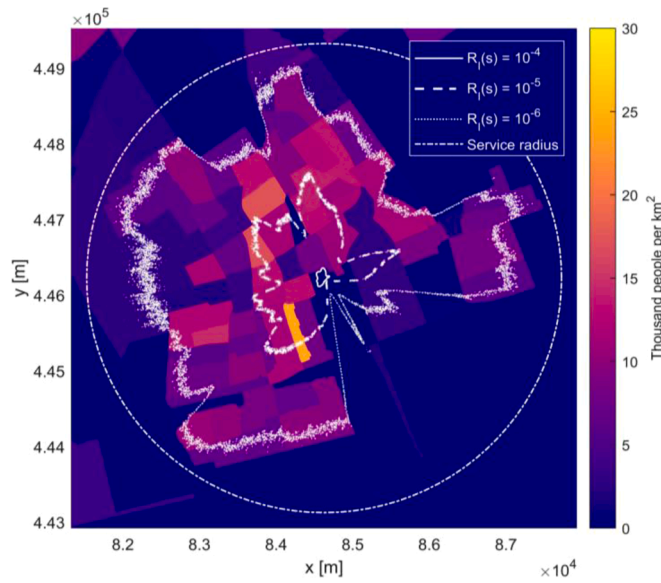
Fig. 8. Individual Risk Contours of $\widehat{R}_I^{UAS}(j) = 10^{-6}, 10^{-5}, 10^{-4}$ projected on population map in Fig. 1.

Table 2
Area and population within individual risk contours in Fig. 8.

Individual Risk contour	% of area	% of population
$\widehat{R}_I^{UAS}(j) > 10^{-6}$	64.5%	81.5%
$\widehat{R}_I^{UAS}(j) > 10^{-5}$	9.0%	13.9%
$\widehat{R}_I^{UAS}(j) > 10^{-4}$	0.1%	0.004%

flights the passing over the 10^{-6} threshold is rather limited, i.e. almost all less than a factor 1.5. In Fig. 6, these flight paths of the UA flights with $\widehat{R}_{Cground}^i / T_i^{nom} > 10^{-6}$ are projected on the population map. These paths fly across an area with relative high population density.

6.3. Estimated collective ground risk per annum

In Step 14, the estimated collective ground risk $\widehat{R}_{Cground}^{UAS} = 0.063$ fatalities per annum for the UAS-based parcel delivery service in the city of Delft. For Step 15, we adopt Eq. (3.5) as threshold. Standing regulation in The Netherlands for airports and hazardous installations [34,35] sets $C = 10^{-3}$ and $\alpha = 2$. This yields a threshold of 0.00165 fatalities per annum, which is 38x lower than the assessed $\widehat{R}_{Cground}^{UAS} = 0.063$ fatalities per annum.

6.4. Estimated individual risk

For Step 7, estimated Individual risk $\widehat{R}_I^{UAS}(j)$ for the considered area is shown in Fig. 7. Because each delivery flight makes a steep climb and a steep descent near the hub, a relative large percentage of UA flight time is near the hub, which leads to the highest value of $\widehat{R}_I^{UAS}(j) = 0.023$ per annum at the hub location. This reflects that the ascend/descent frequency is orders in magnitude higher near the delivery centre than it is at other areas, including the area with the highest population density.

For Step 8 in comparing individual risk $\widehat{R}_I^{UAS}(j)$ to applicable threshold, Fig. 7 projects the 10^{-6}, 10^{-5} and 10^{-4} contours on the surface plot of $\widehat{R}_I^{UAS}(j)$. This shows that for most of the area the threshold

value of 10^{-6} per annum is passed. In Fig. 8, individual risk contours of 10^{-6}, 10^{-5} and 10^{-4} are projected on the population map. This shows that the area within the 10^{-5} contour includes a significant part of the population. Calculated percentages in size and population of the areas within the three contours in Fig. 8 are given in Table 2. This shows that the 10^{-6} individual risk contour includes 81.5% of the population within the delivery area considered. The 10^{-5} individual risk contour includes 13.9% of the population. The 10^{-4} individual risk contour includes 0.004% of the population only (5 persons).

6.5. Discussion of simulation results

For a hypothetical UAS-based parcel delivery service to the population in Delft, three TPR models for UAS operations have been assessed, i. e. Collective ground risk per UA flight hour, Collective ground risk per annum, and Individual risk. In literature on TPR of UAS operations only the Collective ground risk per UA flight hour is assessed. Therefore we first discuss the simulation results obtained for this commonly used model, and subsequently address the results obtained for the two novel TPR models.

If the assessed Collective ground risk per UA flight hour is averaged over all $N = 1,582,985$ UA delivery flights per annum, then it is about a factor 1.5 lower than the applicable threshold of 10^{-6} per flight hour proposed for Europe [3]. However for 31.4% of the individual UA flights the applicable threshold is passed, by at most a factor 1.9. The passing of this threshold does not apply to parcel deliveries by the small UA; it only applies to about 50% of the parcels delivered by the larger UA.

In contrast to the existing Collective ground risk per UA flight hour, the two novel TPR models pose more serious safety obstacles. For the novel TPR indicator Collective ground risk per annum the simulation results show a level that is a factor 38 higher than the standing regulation for airports and hazardous installations [34, 35].

The simulation results for the Individual risk show for most locations, except those near the outer range, assessed $\widehat{R}_I^{UAS}(j)$ values that go beyond the applicable threshold of 10^{-6} probability of fatality per annum due to UA hit of an unprotected person [34,35]. The percentages where this threshold is not satisfied accounts for 64.5% of the area and 81.5% of the population within the considered area. In view of standing regulation in The Netherlands, if this threshold value of 10^{-6} is not satisfied for commercial air traffic around Schiphol, then the following zonal policies have been implemented around the airport. All housing within the 10^{-5} contour have been demolished, all housing development inside the 10^{-6} contour has been banned, and a waiver has been given for the houses in between these two contours. Introducing a similar zonal policy to the hypothetical UAS-based parcel delivery service in Delft would mean that 13.9% of the population in the area has to leave their housing, and that 81.5% - 13.9% = 67.6% of the population a waiver is needed to remain living in their current housing.

A factor 10 improvement in UAS system failure rate would mean that the assessed levels for each of the three TPR indicators go a factor 10 down. For the Individual risk $\widehat{R}_I^{UAS}(j)$ this would mean that the 10^{-6} contour would shrink to the location of the 10^{-5} contour in Fig. 8. Similarly, the 10^{-5} contour would shrink to the location of the 10^{-4} contour in Fig. 8. Hence, only five persons would have their housing within the novel 10^{-5} contour. For the zonal policy this would mean that these 5 persons have to give up their housing and a waiver has to be given for 13.9% of the population to continue living in their houses within the shrinked 10^{-6} contour (9.0 % of area). Even on this basis it will be difficult for Delft to welcome the parcel delivery service considered. In addition, the novel Collective ground risk per annum $\widehat{R}_{Cground}^{UAS}$ would still be a factor 3.8 higher than allowed by standing TPR regulation for airports and hazardous installations.

Because the assessed TPR levels are based on models, instead of statistical data, there is a non-negligible level of uncertainty in these

point estimates. Such uncertainties stem from the following model assumptions:

- Wind does not lead to significant deviation from the nominal flight path.
- There is no general aviation in the airspace used by the UAS flights.
- During uncoordinated descent to the ground other UA's are ignored.
- All crashes to the ground are outcomes of a ballistic descent.
- During ballistic descent there is no tumbling and no rotor wind-milling.
- Buildings and other infrastructure do not influence accident location.
- The Range Commanders Council adopted fatality probability model [44].
- The small size assumption of the crash impact area.
- The estimated percentage of the population that is not sheltered.

Of these model assumptions all except the latter have a similar effect on all three model based TPR assessments. Moreover the sheltering assumption has similar effects on the two Collective risk models. This means that the model assumptions do not have significant effect on the Monte Carlo simulation based comparison of the two novel TPR models versus the existing TPR model.

7. Conclusions

This paper has studied third party risk (TPR) that is posed by commercial use of a UAS operation that consists of a large number of UA flights per annum, e.g. UAS based parcel delivery in an urban area. Under current regulations such commercial UAS operations over an urban area is not allowed. However with the further development of reliable small UA these operations might prove to be sufficiently safe in future, as a result of which future regulations could allow small UA commercial operations over urban areas. From the literature review in Section 2 it has become clear that TPR literature has focused on the risk posed to persons on the ground per UA flight hour. However to manage the future risk of commercial UAS operations over an urban area there is a need for TPR models that capture the risk posed to the population by a large number of UA flights per annum. For commercial aviation the latter has been established through the use of models for Collective ground risk and Individual risk posed to the persons on the ground. Similar model extensions in terms of Individual risk and Collective ground risk for UAS operations have been developed in Section 3. Subsequently, Section 4 has developed a MC simulation method to assess these TPR models.

In Section 5 a scenario of a UAS based parcel delivery service for the city of Delft in The Netherland has been developed. This includes number of parcel deliveries, parcel weights, types of UAs to be used, wind effects, and flight profiles for the parcel deliveries. Subsequently in Section 6 this parcel delivery service scenario has been assessed using the TPR models developed in Section 3 and the MC simulation steps of section 4.

The MC simulation results in Section 6 show that for the hypothetical UAS based parcel delivery service in the city of Delft the existing TPR requirement in terms of expected number of ground fatalities per UA flight hour will largely be satisfied. However the MC simulation results in Section 6 also show that the levels assessed for the two novel TPR models are an order in magnitude higher than standing TPR requirements on airports and hazardous installations.

The overall conclusion is that the two novel TPR indicators fill a gap in understanding third party risk from a population perspective. The novel Collective ground risk per annum accumulates the risk contributions by a large number of UA flights in a rural area. The added value of Individual risk is that it identifies population areas which are posed to relatively high TPR; and therefore supports zonal policies.

The TPR evaluation of a hypothetical application to a UAS based parcel delivery service in the city of Delft shows that from a population

perspective there is a need for substantial further developments in UAS operations. Recently, Petritoli et al. [46] has studied the development of a highly reliable UAS design; the overall reliability of this design is a factor 10 better than the UAS system failure rate assumed in the current simulation study. However overall reliability of a design covers only the technical share of UAS system failures; it does not cover non-technical issues such as human error, unexpected adverse weather, or collision with a bird, a building or with another UA. Hence to realize a factor 10 improvement in UAS system failure rate requires much more than the design by [46] alone. An important development is the mitigation of remaining TPR risks by safety management systems integrated on-board UAs [47,48] and ground-based support [49].

Because the assessed TPR levels are based on models, instead of statistical data, there is a non-negligible level of uncertainty in these point estimates. To reduce this level of uncertainty there is a need for further development in TPR submodels. Each of the uncertainties mentioned in Section 6.5 are valuable candidates for follow-on research. This includes the development of further models for quadcopter non-ballistic descents as well as the development of submodels for non-technical hazards such as human error, unexpected weather change, and mid-air collisions. In [50] Multi-Body System (MBS) modelling and simulation is used to get insight in the validity of the human impact fatality model of [44]. A logical follow-up is to extend this MBS modelling and simulation to better understand the quantification in Eq. (2.8) of the product of the two right hand terms, i.e. size of the crash impact area multiplied by the human fatality probability. Another aspect that deserves further research is that TPR of UAS operations does not only address persons on the ground, though also persons on board of aircraft that are hit by a UA [8,51]. To gain a better understanding [52] has identified the extra TPR terms and which are covered by current regulation and which not. For the studied parcel delivery service in the city of Delft there is need to manage the third party risk posed by fly-away UAS to passengers onboard aircraft to and from Rotterdam The Hague airport, e.g. [53].

Declaration of Competing Interest

The authors declare that they have no known competing financial interests or personal relationshipsthat could have appeared to influence the work reported in this paper.

Acknowledgment

References

[1] ICAO, Unmanned Aircraft Systems (UAS). Circular 328-AN/190. International Civil Aviation Organization; 2011.

[2] FAA. "Operation and certification of small unmanned aircraft systems,". Washington, USA: Department of Transportation; 2016.

[3] JARUS. Guidelines on specific operation risk assessment (SORA). Joint Authorities Regulation Unmanned Systems; 2017.

[4] Bohnenblust H. Risk-based decision making in the transportation sector. In: Jorissen RE, Stallen PJM, editors. Quantified societal risk and policy making. Dordrecht: Kluwer Academic Publishers; 1998.

[5] Ale BJM, Piers M. The assessment and management of third party risk around a major airport. J Hazard Mater January 2000;71(1–3):1–16.

[6] Jonkman SN, Van Gelder PHAJM, Vrijling JK. An overview of quantitative risk measures for loss of life and economic damage. J Hazard Mater 2003;A99:1–30.

[7] Weibel RE, Hansman Jr RJ. "Safety considerations for operation of different classes of UAVs in the NAS,". Unmanned Unlimited. In: Technical conference, workshop and exhibit; 20-23 Sept. 2004. p. 1–11. AIAA-2004-6421.

[8] Clothier R, Walker R. "Determination and evaluation of UAV safety objectives,". In: Proceedings of the 21st international UAV systems conference; 2006. 18.1-18.16.

[9] Dalamagkidis K, Valavanis K, Piegl L. On integrating unmanned aircraft systems into the National Airspace System. 2nd ed. Springer; 2012.

[10] Lum C, Waggoner B. "A risk based paradigm and model for unmanned aerial systems in the national airspace,". In: AIAA conference; 2010.

[11] Melnyk R, Schrage D, Volovoi V, Jimenez H. "A third-party casualty risk model for unmanned aircraft system operations,". Reliab Eng Syst Saf 2014;124:105–16.

[12] Rudnick-Cohen ES, Azarm S, Herrmann J. Multi-objective design and path planning optimization of unmanned aerial vehicles (UAVs). In: 16th AIAA/ISSMO multidisciplinary analysis and optimization conference; 2015.

[13] Rudnick-Cohen E, Herrmann JW, Azarm S. Modeling Unmanned Aerial System (UAS) risks via Monte Carlo simulation. In: 2019 international conference on UAS (ICUAS2019); June 11-14, 2019.

[14] Bertrand S, Raballand N, Viguier F, Muller F. Ground risk assessment for long-range inspection missions of railways by UA's. In: Proceedings of the 2017 international conference on unmanned aircraft systems; 2017.

[15] La Cour-Harbo A. The value of step-by-step risk assessment for unmanned aircraft. In: Proceedings of the 2018 international conference on unmanned aircraft systems (ICUAS); June 2018. p. 149–57.

[16] La Cour-Harbo A. Quantifying risk of ground impact fatalities for small unmanned aircraft. J Intell Robot Syst 2019;93:367–84.

[17] Foster JV, Hartman DC. High fidelity unmanned aircraft system simulation development for trajectory prediction under off-nominal flight dynamics. In: 17th AIAA ATIO conference; 2017.

[18] Cunningham K, Cox DE, Foster JV, Riddick SE, Laughter SA. AirSTAR beyond visual range system description and preliminary test results. AIAA Sci Tech Forum January 2016.

[19] Ancel E, Capristan F, Foster J, Condotta R. Real-time risk assessment framework for UAS traffic management (UTM). In: 17th AIAA ATIO conference; 2017. AIAA-2017-3273.

[20] La Cour-Harbo A. Ground impact probability distribution for small unmanned aircraft in ballistic descent. In: Proceedings of the ICUAS 2020; September 2020.

[21] Primatesta S, Rizzo A, Cour-Harbo ALa. Ground risk map for Unmanned Aircraft in urban environments. J Intell Robot Syst May 2019. https://doi.org/10.1007/s10846-019-01015-z.

[22] Laheij GMH, Post JG, Ale BJM. Standard methods for land-use planning to determine the effects on societal risk. J Hazard Mater 2000;71:269–82.

[23] Christou M, Gyenes Z, Struckl M. Risk assessment in support to land-use planning in Europe: towards more consistent decisions?. J Loss Prevent Process Ind, 24; 2011. p. 219–26.

[24] Smets H. Frequency distribution of the consequences of accidents involving hazardous substances in OECD countries. Etudes et Dossiers: Geneva Association; 1996.

[25] Lum CW, Gauksheim K, Kosel T, McGeer T. Assessing and estimating risk of operating Unmanned Aerial Systems in populated areas. In: 11th AIAA ATIO conference; September 2011. AIAA-2011-6918.

[26] Barr LC, Newman RI, Ancel E, Belcastro CM, Foster JV, Evans JK, Klyde DH. Preliminary risk assessment for small unmanned aircraft systems. In: 17th AIAA ATIO conference; 2017.

[27] Kim SH. Third-Party risk of mid-air collision between small unmanned aircraft systems. In: Proceedings of the AIAA aviation forum; June 2019. 10.25.14/6.2019-3052.

[28] Kim SH. Third-party risk analysis of small unmanned aircraft systems operations. J Aerosp Inf Syst 2020;17:24–35.

[29] La Cour-Harbo A, Schioler H. Probability of low-altitude midair collision between general aviation and unmanned aircraft. Risk Anal 2019;39:2499–513.

[30] Haartsen Y, Aalmoes R, Cheung YS. Simulation of unmanned aerial vehicles in the determination of accident locations. In: IEEE international conference on UAS (ICUAS2016); 2016. p. 993–1002.

[31] Aalmoes R, Cheung YS, Sunil E, Hoekstra JM, Bussink F. A conceptual third party risk model for personal and unmanned aerial vehicles. In: Proceedings of the international conference on UAS, ICUAS2015; June 2015.

[32] Abramowitz M, Stegun IA, editors. Handbook of mathematical functions. National Bureau of Standards; December 1972. 10th printing.

[33] Grimme W. "Modelling and Monte Carlo simulation of third party risk of drones,". MSc thesis. Delft University of Technology; February 2018.

[34] Bottelberghs PH. Risk analysis and safety policy developments in The Netherlands. J Hazard Mater 2000;71:59–84.

[35] Trbojevic VM. Risk criteria in EU. In: Proceedings of the ESREL; 2005. 27-30 June 2005.

[36] CBS. Wijk- en buurtkaart. Centraal Bureau voor de Statistiek; 2017 [Online]. [Accessed 26 01 2019].

[37] Doole M, Ellerbroek J, Hoekstra J. "Drone Delivery - Urban airspace traffic density estimation,". Delft: TU Delft; 2018.

[38] KNMI, Uurgegevens van het weer in Nederland, KNMI, https://projects.knmi.nl/klimatologie/uurgegevens/selectie.cgi. [Accessed 26 01 2019].

[39] Microdrones, "md4-3000: the high-powered VTOL quadrocopter from Microdrones," https://www.microdrones.com/en/drones/md4-3000/. Accessed 26 01 2019.

[40] Sunil E, Ellerbroek J, Hoekstra J. "METROPOLIS – urban airspace design - scenario definition report (D 1.2),". TU Delft; 2014.

[41] Microdrones, "md4-1000: robust and powerful – UAV /drone model from Microdrones," https://www.microdrones.com/en/drones/md4-1000/. [Accessed 26 01 2019].

[42] DJI, "Inspire 2 - Specs," [Online]. Available: https://www.dji.com/nl/inspire-2/specs. [Accessed 26 01 2019].

[43] DOD. "Global positioning system standard position service performance standard,". USA, Washington: Department of Defense; 2008.

[44] Range Commanders Council, Range safety criteria for unmanned air vehicles, rationale and methodology supplement; Supplement to Document 321-00, April 2000.

[45] Feinstein DI, Haugel WF, Kardatzke ML, Weinstock A. Personnel casualty study. Illinois Institute of Technology Research; July 1968. Technical Report Project No. J 6067.

[46] Petritoli E, Leccese F, Ciani L. Reliability and maintenance analysis of unmanned aerial vehicles. Sensors 2018;18. https://doi.org/10.3390/s18093171.

[47] Ippolito CA. Dynamic ground risk mitigating flight control for autonomous small UAS in urban environments. Dallas, Texas: AIAA-Aviation Forum; 17-21 June 2019.

[48] Ancel E, Capristan FM, Foster JV, Condotta RC. In-time non-participant casualty risk assessment to support onboard decision making for autonomous unmanned aircraft. AIAA-Aviation Forum; June 2019.

[49] Pang B, Tan Q, Low KH. A risk-based UAS traffic network model for adaptive urban airspace management. AIAA Aviation Forum; June 2020.

[50] Rattanagraikanakorn B, Blom HAP, Sharpanskykh A, De Wagter C, Jiang C, Schuurman M, Gransden D, Happee R. Modeling and simulating human fatality due to quadrotor UAS impact. AIAA Aviation Forum; June 2020.

[51] Clothier RA, Williams BP, Hayhurst KJ. Modelling the risks remotely piloted aircraft pose to people on the ground. Saf Sci 2018;101:33–47.

[52] Jiang C, Blom HAP, Sharphanskykh A. Third party risk indicators and their use in safety regulations for UAS operations. AIAA Aviation Forum; June 2020.

[53] Wang CHJ, Tan SK, Low KH. Three-dimensional (3D) Monte-Carlo modelling for UAS collision risk management in restricted airport airspace. Aerosp Sci Technol 2020;105(105964):1–13.